JOURNAL OF AIRCRAFT
Vol. 42, No. 1, January–February 2005

Drag Computation and Breakdown in Power-on Conditions

Renato Tognaccini*
University of Naples "Federico II," 80125 Naples, Italy

A thrust–drag accounting system is proposed that makes it possible to calculate installation drag from computational fluid dynamics calculations. Given a numerical solution of the viscous subsonic or transonic flow around an aircraft configuration in power-on conditions, an entropy drag expression is derived. Therefore, a method for the computation and breakdown of the entropy drag in viscous and wave components can be extended and applied to powered configurations. The possibility of identifying spurious contributions improves the accuracy of the drag calculation for a given grid. Two applications are presented: a simple two-dimensional model problem and a transonic flow around an isolated nacelle with core and fan jets.

Nomenclature

A	=	section area of the captured stream tube
C_D	=	drag coefficient
D	=	drag
D_{inf}	=	drag of the infinite body
D_{nac}	=	nacelle drag
$D_{\Delta s}$	=	entropy drag
$D_{\Delta s,\text{nac}}$	=	entropy nacelle drag
$\boldsymbol{e}_x$	=	unit versor of x axis
$\boldsymbol{F}$	=	net propulsive force
F_x	=	x component of net propulsive force
f_{s1}, f_{s2}	=	coefficients of the expansion of the velocity module
$\boldsymbol{I}$	=	total impulse
$\boldsymbol{I}_v$	=	viscous part of total impulse
l	=	reference length
M	=	Mach number
$\dot{m}$	=	mass flux captured by the nacelle
$\boldsymbol{n}$	=	unit vector normal to a surface S, $(n_x, n_y, n_z)^T$
$\hat{\boldsymbol{n}}$	=	unit vector normal to a surface A and directed as the freestream velocity, $(\hat{n}_x, \hat{n}_y, \hat{n}_z)^T$
p	=	static pressure
p_i	=	static pressure in the equivalent ideal flow
p_t	=	stagnation pressure
$\bar{p}$	=	average static pressure in a section of the captured stream tube
R	=	gas constant
Re	=	Reynolds number
Re_D	=	Reynolds number referenced to nacelle diameter
S	=	surface
S'_{in}, S'_{out}	=	particular surfaces in Ω, domain infinitely far from the configuration
S_∞	=	surface enclosing the flow domain infinitely far from the configuration
S'_∞	=	$S_\infty - A_{-\infty} - A_{+\infty}$
s	=	entropy
$\boldsymbol{T}$	=	thrust vector
$\boldsymbol{T}_i$	=	intrinsic net thrust
$\boldsymbol{T}_{\text{ideal}}$	=	ideal net thrust
T_{ix}	=	x component of intrinsic net thrust
$\boldsymbol{T}_o$	=	overall net thrust
T_{ox}	=	x component of overall net thrust
$\boldsymbol{T}_s$	=	standard net thrust
T_{sx}	=	x component of standard net thrust
T_t	=	stagnation temperature
T_x	=	x component of thrust vector
$\hat{\boldsymbol{T}}_o$	=	modified overall net thrust
$\hat{T}_o$	=	x component of modified overall net thrust
$\boldsymbol{U}$	=	unit tensor
V	=	velocity module
$\boldsymbol{V}$	=	velocity vector $(u, v, w)^T$
$\bar{\boldsymbol{V}}$	=	average velocity in section A
$\bar{\boldsymbol{V}}_{i,\text{out}}$	=	ideal velocity obtained by isentropic expansion to atmospheric pressure
x, y, z	=	orthogonal reference system with x axis aligned with freestream velocity
α	=	angle of attack
γ	=	ratio of specific heats
Δs	=	$s - s_\infty$
$\boldsymbol{\Delta T}_{ta}$	=	difference between standard and intrinsic thrust
$\boldsymbol{\Delta T}_{tab}$	=	difference between overall and intrinsic thrust
$(\boldsymbol{\Delta T}_{tab})_i$	=	difference between overall and intrinsic thrust in the equivalent ideal flow
ΔT_{tabx}	=	x component of $\boldsymbol{\Delta T}_{tab}$
$(\Delta T_{tabx})_i$	=	ΔT_{tabx} for the equivalent ideal flow
$(\boldsymbol{\Delta T}_{ta})_i$	=	difference between standard and intrinsic thrust in the equivalent ideal flow
ΔT_{tax}	=	x component of $\boldsymbol{\Delta T}_{ta}$
$\boldsymbol{\Delta T}_{tb}$	=	$\boldsymbol{\Delta T}_{tab} - \boldsymbol{\Delta T}_{ta}$
$\delta \boldsymbol{T}_{tb}$	=	$\boldsymbol{\Delta T}_{tab} - (\boldsymbol{\Delta T}_{tab})_i$
ρ	=	density
$\boldsymbol{\tau}$	=	viscous stress tensor
τ_{xx}, τ_{xy}, τ_{xz}	=	components of $\boldsymbol{\tau}$
Ω	=	flow domain
Ω'	=	subdomain of Ω

Subscripts

body	=	complete nacelle surface including fan inlet, fan outlet, and core outlet
CE	=	core exit
ext	=	external surface of the nacelle
F	=	fan inlet
FE	=	fan exit
far	=	far field
in	=	nacelle inlet
$l\infty$	=	lateral and at infinity
nac	=	nacelle
out	=	nacelle outlet
TE	=	turbine exit
ta	=	upstream tube of captured air
tb	=	downstream tube of captured air
tab	=	upstream and downstream tube of captured air
Δs	=	associated with entropy variation

Received 23 February 2004; revision received 14 April 2004; accepted for publication 15 April 2004.

*Associate Professor, Dipartimento di Progettazione Aeronautica, Piazzale V. Tecchio 80; renato.tognaccini@unina.it.

∞ = freestream value
$-\infty$ = infinitely upstream
$+\infty$ = infinitely downstream

I. Introduction

THE application of computational fluid dynamic (CFD), in particular based on the solution of the Reynolds averaged Navier–Stokes (RANS) equations, is now common practice for the analysis of complete aircraft configurations in power-on conditions.[1,2] However, the possibility to predict drag and thrust by CFD calculations has seen little discussion; the need for such analysis is addressed in Ref. 3, among others. The problem of engine–airframe integration has become even more important for the new generation of very-high and ultrahigh bypass ratio engines. The airplane cruise efficiency improvements resulting from these engines are significantly affected by any installation drag and can be largely negated as a result of suboptimum nacelle–airframe integration.

In flight, the thrust provided by the propulsion system is strongly coupled with the action of the flow on the airframe; it is difficult to separate the thrust and drag contributions to the total force acting on an airplane. Therefore, the identification of an unambiguous definition of the aerodynamic drag in power-on conditions is required.

The problem of drag–thrust bookkeeping is addressed in detail in Refs. 4 and 5, where it is discussed from a general viewpoint: theory, wind-tunnel experiments, in-flight measurements, and ground testing. Very recently, a theoretical analysis that considers CFD applications has been proposed in Ref. 6. In Ref. 4 a clear definition of nacelle drag in power-on conditions has been proposed. It has the interesting feature that it is only associated with dissipative effects: With this definition, the nacelle drag is zero in an inviscid nonlifting flow. However, it has a limited application, even in numerical calculations, because it requires knowledge of the inviscid flow at the same conditions. This nacelle drag definition is a near-field relation in the sense that it relies on integration of the stresses imposed by the flow on the nacelle.

In the present paper, a far-field expression of the nacelle drag is proposed; it can be applied to compute the nacelle drag using the flowfield data obtained by a numerical simulation by a RANS method in the case of power-on conditions, and it allows for a straightforward calculation of the installation drag.

It is also difficult to make an accurate drag prediction from CFD in power-off conditions. Even if an accurate flow solution is available, a reliable drag calculation is challenging, and the breakdown into its components is difficult. Discussion of the progress in this field over the last years may be found in Refs. 7–10. Far-field drag relations, based on integrations of momentum flux on surfaces far from the configurations, have also been applied. Oswatitsch[11] derived a well-known first-order far-field expression in terms of entropy variations in the flowfield (entropy drag), which takes into account viscous and wave contributions. This relation has been applied for drag calculations from RANS numerical solutions as shown, for instance, in Refs. 12–14. Schmitt and Destarac[15] adopted a volume integral formulation of the entropy drag, which has some interesting features (also see Ref. 16): limiting the integration to regions where entropy drag have physical sources (boundary layers, shock waves) strongly reduces the contribution associated with numerical errors and artificial dissipation (spurious drag) and, therefore, makes for improved accuracy for a specified mesh size. Moreover, as proposed in Ref. 17, it is possible to obtain a breakdown of the entropy drag in its physical contributions (viscous and wave drag) once the boundary-layer and shock wave regions are identified in the computational domain.

In what follows, the method proposed in Ref. 17 (also Ref. 18) for the calculation and breakdown of the entropy drag in power-off conditions is briefly illustrated. Then the problem in power-on conditions is addressed. The different thrust definitions, as proposed in Ref. 4, are recalled to formulate a proper thrust–drag bookkeeping system providing an entropy drag expression. This new expression of the nacelle drag allows for extension of the method[17] to the case of power-on conditions, as will be shown in two simple applications in the final part of the paper. Preliminary results of the present work have been proposed in Refs. 18 and 19.

II. Aerodynamic Drag in Power-off Conditions

In a situation of steady subsonic or transonic flow with freestream velocity V_∞ and pressure p_∞ around an unpowered aircraft configuration, the only external force acting on the body is due to the fluid. The integral momentum balance equation makes it possible to define the total aerodynamic force and, in particular, drag by an integration of stresses on the aircraft configuration (near-field expression) or by an integration of momentum flux on a closed surface far from the configuration (far-field expression).

When a Cartesian reference system with the x coordinate aligned with V_∞ is assumed, the far-field expression of drag is given by

$$D_{\text{far}} = -\int_{S_{\text{far}}} [(p - p_\infty)n_x + \rho u(\boldsymbol{V}\cdot\boldsymbol{n})]\,\mathrm{d}S \tag{1}$$

where S_{far} specifies the closed surface far from the configuration, p and $\boldsymbol{V} = (u, v, w)$ are the local pressure and velocity, $\boldsymbol{n} = (n_x, n_y, n_z)$ is the unit vector normal to S_{far} and pointing outward as shown in Fig. 1. In this expression, the viscous stresses have been neglected. As discussed in Ref. 8, this hypothesis is valid as long as the viscous body wake is thin; viscous stresses in the wake could be significant in the case of airfoils in stall and poststall conditions or bluff bodies.

When this expression is expanded in Taylor series with respect to entropy, pressure, and total enthalpy variations, the aerodynamic drag can be split into four contributions (see Ref. 17). The term associated with entropy rise ($\Delta s = s - s_\infty$) is the entropy drag in power-off conditions; it is the direct product of boundary layers and shock waves. For two-dimensional adiabatic flows in turbulent air, entropy drag is the total drag. In the case of three-dimensional lifting flows, the drag induced by the free-vortex system also has to be considered (lift induced or vortex drag); it is mainly associated with the pressure variations in the wake of the wings.[17]

When Ref. 17 is followed, and first- and second-order terms are included, the entropy drag for three-dimensional flows reduces to

$$D_{\Delta s} = -V_\infty \int_{S_{\text{far}}} \left[f_{s1}\frac{\Delta s}{R} + f_{s2}\left(\frac{\Delta s}{R}\right)^2 \right] \rho(\boldsymbol{V}\cdot\boldsymbol{n})\,\mathrm{d}S \tag{2}$$

where R is the gas constant for air, and where the coefficients f_{s1} and f_{s2} depend on the ratio of the specific heats for air, γ, and on the freestream Mach number M_∞:

$$f_{s1} = -\frac{1}{\gamma M_\infty^2}, \qquad f_{s2} = -\frac{1 + (\gamma - 1)M_\infty^2}{2\gamma^2 M_\infty^4} \tag{3}$$

Finally, Eq. (2) can be expressed in divergence form by applying Gauss's theorem in the finite flow domain Ω because on the aircraft surface $\boldsymbol{V}\cdot\boldsymbol{n} = 0$,

$$D_{\Delta s} = -V_\infty \int_\Omega \nabla\cdot\left\{ \rho\left[f_{s1}\frac{\Delta s}{R} + f_{s2}\left(\frac{\Delta s}{R}\right)^2 \right]\boldsymbol{V} \right\} \mathrm{d}\Omega \tag{4}$$

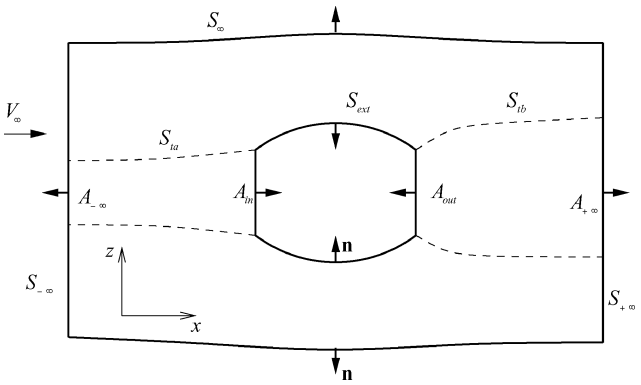

Fig. 1 Flow around an isolated turbojet nacelle.

Relations (2) and (4) define the entropy drag in surface integral and divergence form for both two- and three-dimensional flows, respectively. Oswatitsch's entropy drag expression[11] is recovered by considering only the first-order term in Eq. (2). However, as shown in Ref. 17, the second-order term must be retained in viscous flows because it provides a significant contribution in the boundary-layer region.

The integrand into Eq. (4) is connected with the entropy production rate per unit volume; therefore, viscous and wave drag is produced only in regions where entropy is produced. This property makes the entropy drag relation (4) particularly interesting because it associates drag with its local production. The integrand of Eq. (4) can be defined as the local production rate of entropy drag. Hence, given a single definition of the viscous (boundary layer plus wake) and of the shock wave regions, the entropy drag can be expressed by relation (4) as the sum of three contributions associated with the boundary layer, shock wave region, and remaining part of the flow. In the latter region, for a real flow, entropy drag is not produced. This term (spurious drag) is in general not zero if evaluated using a numerical solution. It is due to the spurious entropy production related to the dissipation of the numerical scheme, discretization errors, and grid stretching. A large spurious entropy production can significantly affect the accuracy of the computed solution, hence, the importance of the studies devoted both to improving the accuracy of numerical schemes and to developing methods for generating high-quality grids. The identification of at least part of the spurious contribution can help to improve the drag prediction. The spurious drag can be nonnegligible, in particular in the case of three-dimensional grids around complex configurations, and is responsible for the difficulty of computing drag by a near-field approach even with a locally accurate CFD result. Note that, in numerical solutions, the entropy production can also be negative: Spurious entropy variations can provide an artificial spurious thrust. This is the case when nonmonotonic schemes are used. Regions with artificial thrust production can be found, in particular, in the shock region, at the border of the boundary layer, or near the far-field boundaries.

III. Thrust–Drag Bookkeeping

When the aircraft configuration to be studied includes thrust by a turbojet or turbofan engine, the body surface S_{body} includes the intakes and outlets of the engines. When the convective momentum flux across the intakes and exhaust jets of the engines is also considered, the momentum balance equation provides the total force acting on the configuration:

$$\boldsymbol{F} = \int_{S_{\text{body}}} [\rho \boldsymbol{V}\boldsymbol{V} + (p - p_\infty)\boldsymbol{U} - \boldsymbol{\tau}] \cdot \boldsymbol{n}\, \mathrm{d}S$$

$$= -\int_{S_{\text{far}}} [\rho \boldsymbol{V}\boldsymbol{V} + (p - p_\infty)\boldsymbol{U} - \boldsymbol{\tau}] \cdot \boldsymbol{n}\, \mathrm{d}S \tag{5}$$

In this expression, the force $\boldsymbol{F}$ is defined by a near-field (first identity) and by a far-field (second identity) integration. Without loss in generality, in what follows the body consists of an isolated turbojet nacelle (single-stream flow) with negligible lift forces. The geometry (Fig. 1) is composed by a nacelle inlet A_{in}, an outlet A_{out}, and an external surface S_{ext}. In Fig. 1, the stream tube of section A is also evidenced, containing the air captured by the nacelle inlet, characterized by the capture area $A_{-\infty}$, and the stream tube defining the exhaust jet with the area $A_{+\infty}$ infinitely downstream. The upstream and downstream lateral surfaces of the stream tube are denoted S_{ta} and S_{tb}, respectively. The surface S_{far} is considered to be infinitely far from the nacelle and built up by two planes perpendicular to the freestream velocity $S_{-\infty}$ and $S_{+\infty}$ connected by a streamlined surface $S_{l\infty}$, where $\boldsymbol{V} \cdot \boldsymbol{n} = 0$ on $S_{l\infty}$. In this case, $\boldsymbol{F}$ is the so-called net propulsive force. The net propulsive force comprises the effective thrust minus the drag due to the action of the flow on the external surface of the nacelle. However, these contributions are coupled and cannot be easily identified. This is the difficulty of defining a correct and unambiguous bookkeeping between thrust and drag. The problem is further complicated for a complete aircraft, when pylons, wing, and fuselage interferences, etc., must also be considered.

When the x component (freestream direction) of $\boldsymbol{F}$ and of the thrust vector $\boldsymbol{T}$ are specified by F_x and T_x, respectively, it is possible to write

$$F_x = T_x + D \tag{6}$$

Thus, the problem of bookkeeping consists in the determination of the drag D when a definition of $\boldsymbol{T}$ has been specified. (With the present definition, T_x is negative in the propulsive case.)

A detailed analysis of all of the general aspects of the problem (definitions, experimental setup, flight testing, etc.) may be found in Refs. 4 and 5. The main goal here is to look for an unambiguous split between thrust and drag of the net force acting on the configuration that can be suitable for CFD applications. It would be very attractive to express this drag in terms of entropy variations, that is, entropy drag, to extend the drag breakdown procedure, already proposed in Ref. 17, to the case of configurations with engine installed and power-on conditions.

This is no simple task. The first question to arise is how to bookkeep the dissipative effects in the wake of the fan and core jets.

It seems reasonable to insert these phenomena into the thrust variations due to real flow effects (viscosity). Indeed the bookkeeping should already be done as thrust in the experimental measurements of the thrust. The problem now is how to proceed when what should be an accurate numerical solution of the RANS equations with power-on conditions is available in the complete flow domain.

Once the drag in the power-on condition is available, the installation drag can be computed by subtracting from this term the drag computed for the wing–body–tail configuration.

In Ref. 4 (p. 27), a number of requirements for an effective practical bookkeeping system have been identified. Basically the need is addressed for avoiding ambiguities and for identifying the regions of responsibilities of the airframe and engine manufacturers.

The present paper focuses on the analysis of the aerodynamic drag in a well-defined thrust–drag bookkeeping system, and thrust computations from CFD calculations will be not discussed. Nonetheless, the aerodynamic drag definition in power-on conditions requires a preliminary survey of the thrust definitions adopted in literature.

Thrust (net thrust) is usually defined as the difference between the total impulse (gross thrust) evaluated in two different stations of the stream tube crossing the nacelle duct. The total impulse $\boldsymbol{I}$ is given by

$$\boldsymbol{I} = \int_A [\rho \boldsymbol{V}\boldsymbol{V} + (p - p_\infty)\boldsymbol{U} - \boldsymbol{\tau}] \cdot \hat{\boldsymbol{n}}\, \mathrm{d}S = \dot{m}\bar{\boldsymbol{V}} + (\bar{p} - p_\infty)A\hat{\boldsymbol{n}} + \boldsymbol{I}_v \tag{7}$$

where $\dot{m}$ is the mass flux,

$$\dot{m} = \int_A \rho \boldsymbol{V} \cdot \boldsymbol{n}\, \mathrm{d}S$$

$\bar{\boldsymbol{V}}$ and $\bar{\boldsymbol{p}}$ are the average velocity and pressure on A, respectively, $\hat{\boldsymbol{n}}$ is the unit vector normal to A and directed as the freestream velocity. $\boldsymbol{I}_v$ specifies the impulse contribution due to the viscous stresses, which is negligible in the stream tube upwind of the nacelle inlet (where there is no boundary layer) and even in the downwind tube, where a boundary layer is developed, if the surface A is perpendicular to the main flow direction. Air spillage inside the engine and fuel mass are here (as usual) neglected, and $\dot{m}$ is assumed constant along the stream tube.

Different thrust definitions are used in the literature depending on the stations chosen for the impulse evaluation. A comprehensive description is given in Ref. 4, and they are briefly referred to here.

The intrinsic net thrust is defined by adopting as interfaces A_{in} and A_{out}:

$$\boldsymbol{T}_i = \int_{A_{\text{in}}} [\rho \boldsymbol{V}\boldsymbol{V} + (p - p_\infty)\boldsymbol{U} - \boldsymbol{\tau}] \cdot \hat{\boldsymbol{n}}\, \mathrm{d}S$$

$$- \int_{A_{\text{out}}} [\rho \boldsymbol{V}\boldsymbol{V} + (p - p_\infty)\boldsymbol{U} - \boldsymbol{\tau}] \cdot \hat{\boldsymbol{n}}\, \mathrm{d}S \tag{8}$$

If the momentum balance equation is written for the flow domain inside the nacelle (from the nacelle inlet to the nacelle outlet), it is possible to derive the force exerted by the fluid on the internal walls of the nacelle duct and simple to show that it is equal to the intrinsic net thrust. In practice, however, this is not a convenient definition because thrust is, in this case, strongly dependent on the intake geometry and on the flow conditions that identify the stagnation line at the nacelle lip, and in addition, the surface A_{in}.

This limitation is removed if $A_{-\infty}$ is adopted instead of A_{in} because the capture area, at a given velocity and altitude, only depends on $\dot{m}$, which is the parameter defining the engine working conditions. In this way, the standard net thrust definition is obtained:

$$\boldsymbol{T}_s = \int_{A_{-\infty}} \rho \boldsymbol{V}\boldsymbol{V}\cdot\hat{\boldsymbol{n}}\,\mathrm{d}S - \int_{A_{\text{out}}} [\rho \boldsymbol{V}\boldsymbol{V} + (p-p_\infty)\boldsymbol{U} - \boldsymbol{\tau}]\cdot\hat{\boldsymbol{n}}\,\mathrm{d}S \quad (9)$$

In the engine design conditions, the mass flow ratio (MFR) $= A_{-\infty}/A_{\text{in}}$ is equal to one, and because $\boldsymbol{\tau}$ can be neglected in the momentum balance applied to the upwind stream tube, intrinsic and standard net thrusts are seen to be equal.

If A_{out} is substituted by $A_{+\infty}$, the overall net thrust definition is obtained:

$$\boldsymbol{T}_o = \int_{A_{-\infty}} \rho \boldsymbol{V}\boldsymbol{V}\cdot\boldsymbol{n}\,\mathrm{d}S - \int_{A_{+\infty}} [\rho \boldsymbol{V}\boldsymbol{V} - \boldsymbol{\tau}]\cdot\boldsymbol{n}\,\mathrm{d}S \quad (10)$$

In a real viscous flow, due to the momentum diffusion, $\boldsymbol{T}_o$ is difficult to evaluate because as the downwind interface is moved infinitely far from the configuration $V \to V_\infty$ and $A_{+\infty} \to \infty$. Moreover, the stream tube S_{T_b} can be clearly defined only in the case of inviscid or laminar flow because, in the turbulent case, the mass entrainment due to the turbulent diffusion has to be considered. However, the exhaust jet can be well approximated for many nacelle lengths by an inviscid contact discontinuity. Thus, instead of the usual standard net thrust definition, it is common practice to apply the ideal net thrust

$$\boldsymbol{T}_{\text{ideal}} = -\dot{m}(\bar{\boldsymbol{V}}_{i,\text{out}} - \boldsymbol{V}_\infty) \quad (11)$$

where $\bar{\boldsymbol{V}}_{i,\text{out}}$ is the ideal speed obtained infinitely far downstream by considering an isentropic expansion of the exhaust jet to atmospheric pressure. In the ideal expression (11) there are two approximations.

1) The boundary layers in the exhaust jets (two jets are present in a two-stream engine) are not considered.

2) The fan and core nozzles often work in choked conditions with a significant external expansion and formations of complex shock patterns, so that the postexit expansion is far from being isentropic even assuming an inviscid flow.

Another thrust definition can be obtained by considering the impulses evaluated at the fan inlet and turbine exit. This definition would simplify the work of the aerodynamicist because these interfaces are usually the boundaries of the flow domain adopted in the numerical aerodynamic analysis where the boundary conditions of inlet and outlet are imposed. A straightforward near-field drag definition could be obtained by integrating viscous and pressure stresses on all of the solid boundaries of the domain. However, this definition does not provide a good thrust–drag accounting system because the responsibilities of the engine and airframe manufacturers are generally separated by specifying as the competence of the engine manufacturer what is happening inside the stream tube of the area captured by the engine and leaving to the airframe manufacturer the responsibility for the external flow.

The momentum balance applied to the stream tubes makes it possible to express each thrust definition in terms of the others. Denote

$$\Delta\boldsymbol{T}_{ta} = \int_{S_{ta}} [(p-p_\infty)\boldsymbol{U} - \boldsymbol{\tau}]\cdot\boldsymbol{n}\,\mathrm{d}S \quad (12)$$

$$\Delta\boldsymbol{T}_{tb} = \int_{S_{tb}} [(p-p_\infty)\boldsymbol{U} - \boldsymbol{\tau}]\cdot\boldsymbol{n}\,\mathrm{d}S \quad (13)$$

$$\Delta\boldsymbol{T}_{tab} = \Delta\boldsymbol{T}_{ta} + \Delta\boldsymbol{T}_{tb} \quad (14)$$

The following relations are obtained:

$$\boldsymbol{T}_s = \boldsymbol{T}_i + \Delta\boldsymbol{T}_{ta}, \qquad \boldsymbol{T}_o = \boldsymbol{T}_i + \Delta\boldsymbol{T}_{tab} \quad (15)$$

Then Eq. (5) with definition (8), due to Eqs. (15), leads to

$$\boldsymbol{F} = \boldsymbol{T}_i + \int_{S_{\text{ext}}} [(p-p_\infty)\boldsymbol{U} - \boldsymbol{\tau}]\cdot\boldsymbol{n}\,\mathrm{d}S \quad (16)$$

$$= \boldsymbol{T}_s + \int_{S_{\text{ext}}} [(p-p_\infty)\boldsymbol{U} - \boldsymbol{\tau}]\cdot\boldsymbol{n}\,\mathrm{d}S - \Delta\boldsymbol{T}_{ta} \quad (17)$$

$$= \boldsymbol{T}_o + \int_{S_{\text{ext}}} [(p-p_\infty)\boldsymbol{U} - \boldsymbol{\tau}]\cdot\boldsymbol{n}\,\mathrm{d}S - \Delta\boldsymbol{T}_{tab} \quad (18)$$

It is natural to associate drag with dissipative effects, that is, drag should be zero in a subsonic, nonlifting, inviscid flow. This result can be achieved by introducing p_i, the pressure field of the equivalent ideal flow ($\boldsymbol{\tau} = 0$), which is the nonlifting inviscid flow around the same nacelle geometry, with the same freestream and engine working conditions. The concept of equivalent ideal flow makes it possible to define the nacelle drag as

$$D_{\text{nac}} = \int_{S_{\text{ext}}} \{[(p-p_i)\boldsymbol{U} - \boldsymbol{\tau}]\cdot\boldsymbol{n}\}\cdot\boldsymbol{e}_x\,\mathrm{d}S \quad (19)$$

which is zero for $p = p_i$ and $\boldsymbol{\tau} = 0$.

When Eq. (16) is projected on the x axis, with the help of definition (19) it is possible to verify that

$$F_x = T_{ix} + D_{\text{nac}} + \int_{S_{\text{ext}}} (p_i - p_\infty)n_x\,\mathrm{d}S \quad (20)$$

$$F_x = T_{sx} + D_{\text{nac}} + \int_{S_{\text{ext}}} (p_i - p_\infty)n_x\,\mathrm{d}S - \Delta T_{tax} \quad (21)$$

$$F_x = T_{ox} + D_{\text{nac}} + \int_{S_{\text{ext}}} (p_i - p_\infty)n_x\,\mathrm{d}S - \Delta T_{tabx} \quad (22)$$

All of these equations contain buoyancy terms, that is, related to pressure, in addition to thrust and drag; they do not seem appropriate for a thrust–drag accounting system in which thrust and drag are the only terms. The scope of the present paper is in fact to identify a different thrust–drag accounting system based on these terms.

An important property of the equivalent ideal flow is

$$\int_{S_{ta}} (p_i - p_\infty)n_x\,\mathrm{d}S + \int_{S_{\text{ext}}} (p_i - p_\infty)n_x\,\mathrm{d}S + \int_{S_{tb}} (p_i - p_\infty)n_x\,\mathrm{d}S = 0 \quad (23)$$

which is the famous paradox of D'Alembert for an infinite streamlined body. It is not obvious that this relation, as shown by Prandtl (Ref. 20, p. 195), still holds even if $A_{-\infty} \neq A_{+\infty}$ provided that $\mathrm{d}A/\mathrm{d}x \to 0$ for $x \to -\infty$ and $x \to +\infty$.

A corollary of relation (23), which will be used later, is

$$\int_{S_{l\infty}} (p_i - p_\infty)n_x\,\mathrm{d}S = 0 \quad (24)$$

It can be simply obtained by considering the mass and momentum conservation equations applied to the domain outside the infinite stream tube.

Equation (23) implies that

$$\int_{S_{\text{ext}}} (p_i - p_\infty)n_x\,\mathrm{d}S - (\Delta T_{tabx})_i = 0 \quad (25)$$

where $(\Delta T_{tabx})_i$ is ΔT_{tabx} for the equivalent ideal flow. Thus, the thrust definition best suited for a drag accounting system is the

overall net thrust. In fact, from Eq. (22) applied to the equivalent ideal flow, it provides

$$F_x = T_{ox} \tag{26}$$

that is, in an inviscid flow around an isolated nacelle (no dissipative effects) the only acting force is the overall net thrust. On the contrary, with the other thrust definitions, the buoyancy terms do not cancel out.

On the upstream stream tube surface S_{ta}, the viscous stresses are clearly negligible, so that $\Delta \boldsymbol{T}_{ta}$ is only due to the action of $(p - p_\infty)$ and is equal to $(\Delta \boldsymbol{T}_{ta})_i$ of the equivalent ideal flow.

In addition, when a nacelle nozzle working in design conditions (i.e., with the nozzle exit pressure $p_{\text{out}} = p_\infty$ and uniform pressure field in the jet) is considered first, the momentum balance equation shows that the total impulse across a plane orthogonal to the jet is constant. Viscous and Reynolds stresses only cause the diffusion of the momentum through the boundary layer of the jet wake. For flows at large Reynolds numbers, the effect of the dynamic viscosity in the jet is negligible. The internal energy flux across a plane orthogonal to the jet is also constant, although the large turbulence of the jet causes a production of turbulent kinetic energy compensated by a reduction of the kinetic energy of the mean flow.

In summary, in design conditions for the nozzle, $\Delta \boldsymbol{T}_{tab} = (\Delta \boldsymbol{T}_{tab})_i$ can be assumed even if the surface S_{tb} has not been identified. Then Eq. (22) reduces to

$$F_x = T_{ox} + D_{\text{nac}} \tag{27}$$

Once again, a proper thrust–drag accounting system has been obtained. In this case, in particular, overall and standard net thrust are equivalent. This is not true, in general, if the pressure field is not uniform in the jet, as when the nozzle is working in off-design conditions. Even if the boundary-layer effects can be expected to be of second order, a nonisentropic postexit expansion can be expected, implying that

$$\Delta \boldsymbol{T}_{tab} = (\Delta \boldsymbol{T}_{tab})_i + \delta \boldsymbol{T}_{tb} \tag{28}$$

with $\delta \boldsymbol{T}_{tb} = \Delta \boldsymbol{T}_{tb} - (\Delta \boldsymbol{T}_{tb})_i$. The buoyancy terms in Eq. (22) do not cancel anymore. However these real flow effects can be accounted for as a thrust loss; therefore, a modified overall net thrust definition can be introduced:

$$\hat{\boldsymbol{T}}_o = \boldsymbol{T}_o - \delta \boldsymbol{T}_{tb} \tag{29}$$

This definition is equivalent to the ideal net thrust $\boldsymbol{T}_{\text{ideal}}$ if the boundary-layer effects of the jet and nonisentropic inviscid effects for choked nozzles are neglected. With this definition the force balance,

$$F_x = \hat{T}_{ox} + D_{\text{nac}} \tag{30}$$

is recovered, and a proper and general thrust–drag bookkeeping system is obtained for a real flow, too. In addition, the ambiguity in the definition of the overall net thrust for real flows is solved. Indeed, an indirect evaluation of $\hat{\boldsymbol{T}}_o$ can be obtained by

$$\hat{\boldsymbol{T}}_o = \boldsymbol{F} - D_{\text{nac}} \boldsymbol{e}_x \tag{31}$$

or according to the far-field expression in Eq. (5) applied to the domain in Fig. 1 and when relation (24) is taken into account ($p = p_i$ on $S_l' \infty$)

$$\hat{\boldsymbol{T}}_o = \int_{S_{-\infty}} \rho \boldsymbol{V}\boldsymbol{V} \cdot \hat{\boldsymbol{n}} \, \mathrm{d}S - \int_{S_{+\infty}} [\rho \boldsymbol{V}\boldsymbol{V} - \boldsymbol{\tau}] \cdot \hat{\boldsymbol{n}} \, \mathrm{d}S - D_{\text{nac}} \boldsymbol{e}_x \tag{32}$$

The modified overall net thrust is consistent with a typical technique adopted for the experimental determination of thrust by the engine manufacturer (Ref. 5, pp. 68–71). It consists in injecting the mass flux $\dot{m}$ in the engine compressor by a bellmouth simulating the upwind stream tube. The engine exhaust jet is accurately measured as the input $\dot{m}$. Because the external velocity is zero, there is no action of the fluid on the external surfaces of the engine, that is, the nacelle drag is zero and the measured variation of momentum corresponds to the modified overall net thrust.

IV. Entropy Drag in Power-on Conditions

The bookkeeping equation (30) can give useful applications only if D_{nac} can be simply determined. This is not the case if the nacelle drag definition (19) is used (where knowledge of both real and equivalent ideal fields would be required), and so it is useful to look for alternative computations of this term.

As shown in the preceding section, the jet boundary layer can be responsible for a thrust loss and not for the nacelle drag. That is, the nacelle drag does not change even if the jet is inviscid: It can be computed by neglecting the viscous stresses on S_{ta} and S_{tb}.

When the infinite streamlined body built up by the stream tubes S_{ta}, S_{tb} and by S_{ext} with $\boldsymbol{\tau} \neq 0$ only on S_{ext} is considered, the drag of this body is

$$D_{\text{inf}} = \int_{S_{ta}} (p_i - p_\infty) n_x \, \mathrm{d}S + \int_{S_{tb}} (p_i - p_\infty) n_x \, \mathrm{d}S + \int_{S_{\text{ext}}} [(p - p_\infty) n_x - (\tau_{xx} n_x + \tau_{xy} n_y + \tau_{xz} n_z)] \, \mathrm{d}S \tag{33}$$

Because of definition (19) of D_{nac} and because of D'Alembert paradox (23), Eq. (33) reduces to $D_{\text{inf}} = D_{\text{nac}}$. Furthermore, the far-field drag expression (1) for the infinite streamlined body reduces to

$$D_{\text{nac}} = -\int_{S_\infty'} \rho V (\boldsymbol{V} \cdot \boldsymbol{n}) \, \mathrm{d}S \tag{34}$$

where $S_\infty' = S_\infty - A_{-\infty} - A_{+\infty}$. In this case, the buoyancy term vanishes because of Eq. (24). It is now possible to obtain the expression of the entropy drag for an isolated nacelle following exactly the derivation proposed in the case of unpowered configurations:

$$D_{\Delta s,\text{nac}} = -V_\infty \int_{S_\infty'} \left[f_{s1} \frac{\Delta s}{R} + f_{s2} \left(\frac{\Delta s}{R} \right)^2 \right] \rho (\boldsymbol{V} \cdot \boldsymbol{n}) \, \mathrm{d}S \tag{35}$$

Because the flow has been considered viscous on S_{ext} only, Δs can be other than zero only in the domain Ω' defined by S_{ext}, S_{in}', S_{out}', and $S_{l\infty}$ (Fig. 2). In addition, by the application of the Gauss theorem,

$$D_{\Delta s,\text{nac}} = -V_\infty \int_{\Omega'} \boldsymbol{\nabla} \cdot \left\{ \rho \left[f_{s1} \frac{\Delta s}{R} + f_{s2} \left(\frac{\Delta s}{R} \right)^2 \right] \boldsymbol{V} \right\} \mathrm{d}\Omega \tag{36}$$

In this case also, the force contribution associated with total enthalpy variations[17] is negligible outside the fan and core jets, so that the entropy drag, as defined by Eq. (36), is equal to the nacelle drag D_{nac}.

The entropy production in Ω' can be due to the boundary layer on S_{ext} or to shock waves: Again the nacelle drag can be decomposed in viscous and wave contributions by identifying the boundary layer and the possible shock region near the nacelle surface S_{ext}.

The definition of nacelle drag can be easily extended to the case of two-stream engines. In this case, the surface S_{ext} is defined by

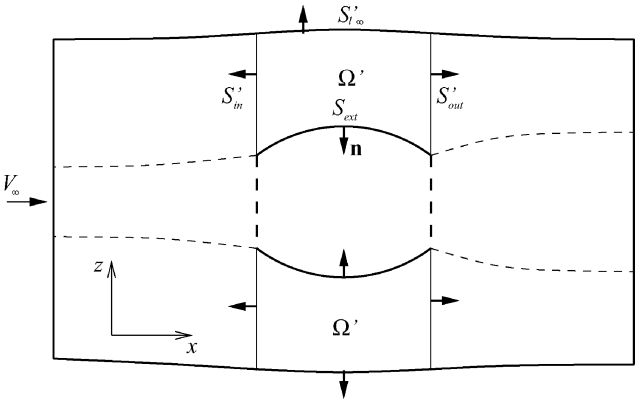

Fig. 2 Domain adopted for computation of the nacelle drag.

the fan cowl only, that is, the action of pressure and viscous forces on the core cowl and core plug contributes to thrust loss and not drag. In accordance with Ref. 5, the action of stresses on the pylon surface immersed in the fan jet should also be accounted for as thrust loss.

The application to complex aircraft configurations (wing–body–pylon–nacelle) is straightforward. Indeed, once the engine jet regions and the zone between the nacelle inlets and fan surfaces are excluded from the volume integration, relation (36) is equivalent to the entropy drag in power-off conditions equation (4). The obtained value is the entropy drag contribution to the total aerodynamic drag in power-on conditions.

V. Applications

A. Simple Model Problem

The flow simulations have been obtained solving the steady RANS equations by a standard technique based on the well-known central space discretization, with self-adaptive explicit second- and fourth-order artificial dissipation,[21] the adopted flow solver being multiblock structured.[22]

The first test case to validate the present analysis is a simple two-dimensional nacelle consisting of two parallel plates of length $3l$ with l the inlet width (Fig. 3). The fan inlet area (A_F) and turbine exit area (A_{TE}) are equal, $A_F = A_{\mathrm{TE}} = A_{\mathrm{in}} = A_{\mathrm{out}}$. If the MFR $= A_{-\infty}/A_{\mathrm{in}}$ is equal to one, the equivalent ideal pressure field is uniform, $p_i = p_\infty$ in the complete flow domain and the nacelle drag, as defined by relation (19), is obtained by integrating the viscous stresses on the external surfaces of the nacelle, that is, the nacelle drag is given by the friction drag on the external surfaces of the two flat plates of length $3l$.

The very simple Cartesian grid is made up of 51,200 cells in the fine-grid level, and the adopted turbulence model is Baldwin–Lomax.[23] Freestream conditions are $M_\infty = 0.5, \alpha = 0$ deg, and $Re_l = 1 \times 10^6$; inlet conditions are MFR $= 1$, $p_{\mathrm{in}}/p_\infty = 1$. Power-off conditions were preliminarily tested: $p_{t_{\mathrm{TE}}}/p_{t\infty} = 1$ and $T_{t_{\mathrm{TE}}}/T_{t\infty} = 1$, where p_t and T_t, respectively, specify stagnation pressure and stagnation temperature.

In Fig. 4, near-field and far-field drag calculations, performed on three grid levels, are compared. The near-field drag has been computed by integrating pressure and viscous stresses on all of the walls of the configuration (including internal walls). Far-field drag has been computed by applying relation (4) to the boundary-layer region selected, including wake (Fig. 5). Drag calculations, repeated by excluding the selected wake, provided the same result, that is, the wake did not contribute to drag (at least in this case). On the finest grid, near-field and far-field drag coefficients are in agreement; far-field drag sensitivity to the grid size is very small. On the contrary, near-field drag proved very sensitive to the grid density. This is due to the poor accuracy of the computation of the velocity derivatives at the wall because of the very small number of grid cells in the boundary layer in the coarse grids.

Power-on conditions were tested by modifying the boundary conditions at the turbine exit: $p_{t_{\mathrm{TE}}}/p_{t\infty} = 1.17$ and $T_{t_{\mathrm{TE}}}/T_{t\infty} = 2.053$. These conditions preserved the conservation of mass across the engine. In these conditions, the ideal thrust is $T_{x_{\mathrm{ideal}}} = 0.8814\rho_\infty V_\infty^2 l$; the nozzle conditions are not choked ($M_{\mathrm{out}} = 0.7$), and there is no postexit expansion.

As already stated, for this particular case the nacelle drag can be computed by integrating viscous stresses on the external walls. Moreover, Eq. (36) has been used for computing the far-field nacelle drag; the spurious contribution has been eliminated limiting the volume integration to the boundary-layer region selected around the external surface of the nacelle shown in Fig. 6. In Fig. 7 far-field and near-field nacelle drag are compared for two grid levels. (In this case the solution on the coarser grid did not converge.) In Fig. 7, the value of the nacelle drag coefficient is also specified, obtained by using Prandtl's relation for the drag of a flat plate (Ref. 24, p. 599), which is 73 counts. On the finest grid, near-field and far-field calculations are in reasonable agreement; again the sensitivity to the mesh size of the far-field calculations is much lower. The agreement with Prandtl's relation is also satisfactory.

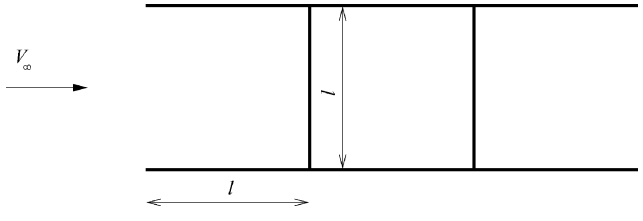

Fig. 3 Geometry of the flat nacelle.

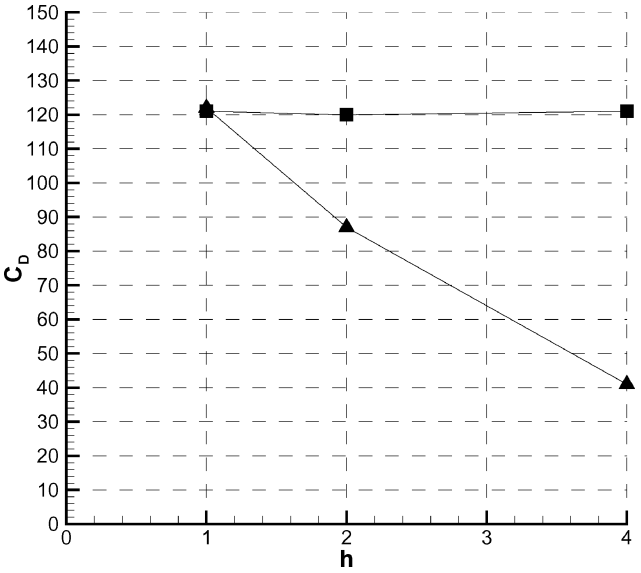

Fig. 4 Flat nacelle test, drag coefficient vs mesh size, $M_\infty = 0.5$, $\alpha = 0$ deg, and $Re_l = 1 \times 10^6$, power-off condition: ▲, near field and ■, far field.

Fig. 5 Boundary-layer region selected for computation of the nacelle drag in flat nacelle test, $M_\infty = 0.5$, $\alpha = 0$ deg, and $Re_l = 1 \times 10^6$, power-off condition.

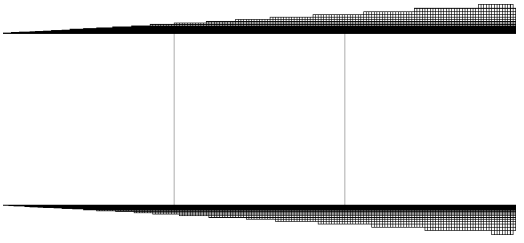

Fig. 6 Boundary-layer region selected for computation of the nacelle drag in flat nacelle test, $M_\infty = 0.5$, $\alpha = 0$ deg, and $Re_l = 1 \times 10^6$, power-on condition.

B. Isolated Turbofan Nacelle

The second test is a more realistic configuration: The geometry is the two-stream turbopowered simulator (TPS) nacelle studied experimentally and numerically during the Engine Integration in Future Transport Aircraft Research Program funded by the European Commission. The flow conditions are $M_\infty = 0.75$, $\alpha = 0$ deg, $Re_\infty = 4.8 \times 10^6$, and MFR $= 0.822$; at the fan exit, $p_{t_{\mathrm{FE}}}/p_{t\infty} = 2.24$ and $T_{t_{\mathrm{FE}}}/T_{t\infty} = 1.13$, and at the core exit, $p_{t_{\mathrm{CE}}}/p_{t\infty} = 1.79$ and $T_{t_{\mathrm{CE}}}/T_{t\infty} = 0.598$. Fan and core jets are both

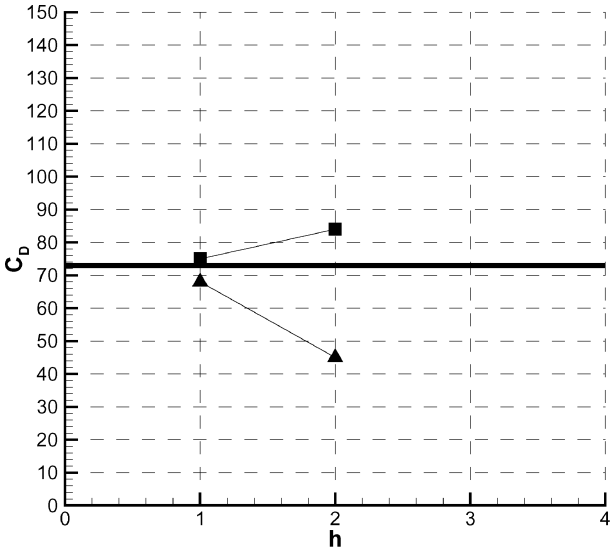

Fig. 7 Flat nacelle test, drag coefficient vs mesh size, $M_\infty = 0.5$, $\alpha = 0$ deg, and $Re_l = 1 \times 10^6$, power-on condition: ▲, near field; ■, far field; and ——, Prandtl's relation.

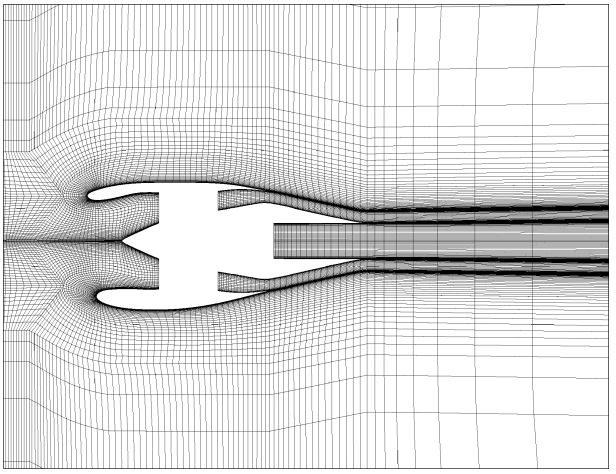

Fig. 8 Partial view of grid in the symmetry plane adopted for simulation of the TPS nacelle configuration.

cold because in a TPS experimental setup, fan and core jets are simulated by external pressurized cold air. The computational grid in the symmetry plane, made up by 210,000 grid cells is shown in Fig. 8. Flow calculations were performed by adopting the Spalart–Allmaras turbulence model.[25]

The obtained iso-Mach contour in power-on conditions is shown in Fig. 9; the stream tube of the flow captured by the fan is also displayed. In these conditions, there are no shocks or supersonic regions in the flow outside the stream tube. On the contrary, both the fan nozzle and core nozzle work in choked conditions with postexit supersonic expansion.

The nacelle drag has been computed by relation (36) applied to the domain (the boundary layer region on the fan cowl) proposed in Fig. 10. By the use, as reference area, of the wing surface of the configuration where the TPS model was mounted (wing–body–pylon–nacelle), $C_{D_{\Delta s,\mathrm{nac}}} = 15$ counts. This value can be a guess of the installation drag for an "ideal" engine–airframe integration. (Indeed, the drag due to the nacelle pylon and the interference effects is not taken into account.) This result is in agreement with the installation drag computed in Ref. 3, as far as a comparison with calculations performed on a completely different configuration (wing–body–nacelle–pylon) makes sense. In Ref. 3, the installation drag was computed as the difference between the near-field drag computed in power-on conditions on the wing–body–pylon–nacelle configuration and in power-off conditions on the wing–body configuration. A small reduction of the lift-induced drag in the case of installed engines could compensate for the friction drag added by the pylon.

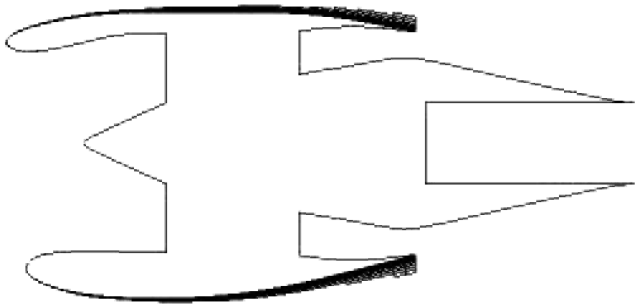

Fig. 10 Boundary-layer region selected for computation of the nacelle drag in the TPS nacelle test, $M_\infty = 0.75$, $\alpha = 0$ deg, and $Re_D = 4.8 \times 10^6$, power-on condition.

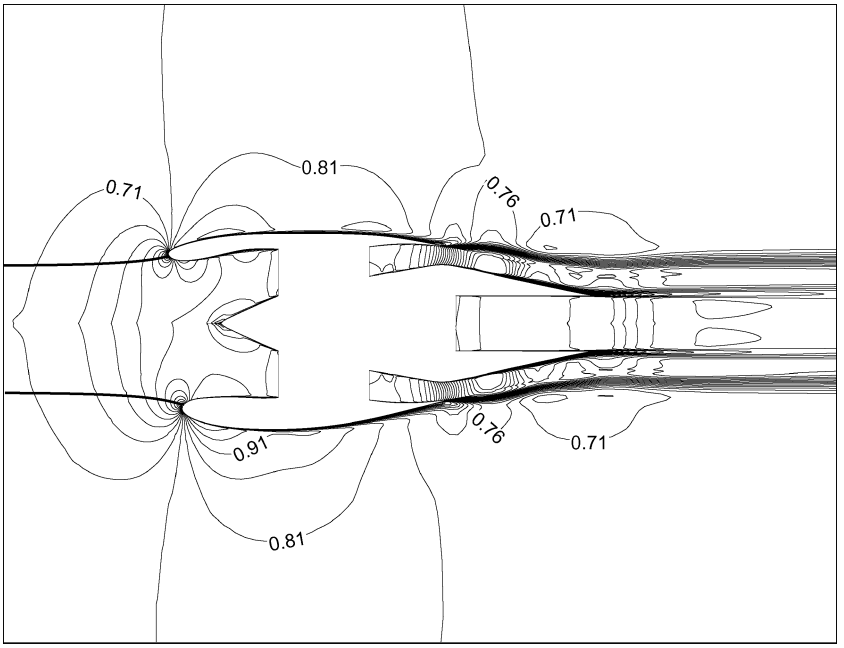

Fig. 9 Iso-Mach contours around the TPS nacelle configuration, $\Delta M = 0.01$; $M_\infty = 0.75$, $\alpha = 0$ deg, and $Re_D = 4.8 \times 10^6$, power-on condition.

VI. Conclusions

A thrust–drag accounting system has been proposed in which the defined aerodynamic drag is suitable for calculation by numerical solutions of the RANS equations. The drag contribution due to the propulsion system is zero if the physical dissipative terms are neglected. The near-field definition would require knowledge of the equivalent ideal flow and is not feasible in practical applications. However, the far-field definition proposed here has been related to the entropy production around the external surfaces of the nacelle; in this way, it has been possible to extend to power-on conditions a method of drag prediction and decomposition already developed for unpowered configurations.

The application of the method has been shown for a simple model problem and for the case of an isolated turbofan nacelle in transonic flow conditions.

Acknowledgments

The present work has been partially developed in the frame of the Aircraft Drag and Thrust Analysis Research Project funded by the European Commission (Contract BPR-C197-470). This paper relies on the invaluable help of Luigi Paparone who performed all of the flow calculations at the Italian Aerospace Research Centre.

References

[1]Hoheisel, H. (ed.), "Aspects of Engine-Airframe Integration for Transport Aircraft," *Proceedings of the DLR Workshop*, German Aerospace Research Center, DLR, Brunswick, Germany, 1996.

[2]Burgsmuller, W., Rollin, C., and Rossow C., "Engine Integration in Future Transport Aircraft—The European Research Programs DUPRIN/ENIFAIR," 21st International Council of the Aeronautical Sciences, Conf., ICAS Paper 98-5.6.1, 1998.

[3]Laban, M., "Aircraft Drag and Thrust Analysis (AIRDATA) Project Overview and Key Results," *Proceedings of the Workshop on EU—Research on Aerodynamic Engine/Aircraft Integration for Transport Aircraft*, German Aerospace Research Center, DLR, Brunswick, Germany, 2000, pp. 9-1, 9-15.

[4]Ministry-Industry Drag Analysis Panel Study Group, "Guide to In-Flight Thrust Measurement of Turbojets and Fan Engines," AGARD-AG-237, Jan. 1979, p. 27.

[5]Covert, E. (ed.), *Thrust and Drag: Its Prediction and Verification*, Vol. 96, Progress in Astronautics and Aeronautics, AIAA, New York, 1985, pp. 68–71.

[6]van der Vooren, J., and Destarac, D., "Drag/Thrust Analysis of Jet-Propelled Transonic Transport Aircraft; Definition of Physical Drag Components," *Aerospace Science and Technology* (to be published).

[7]Deconinck, H., Sermeus, K., and van Dam, C. (eds.), *CFD-Based Aircraft Drag Prediction and Reduction*, LS 2003-02, von Karman Inst. for Fluid Dynamics Lecture Series, von Karman Inst. for Fluid Dynamics, Rhode St-Genese, Belgium, 2003; also National Inst. of Aerospace, Hampton, VA, Nov. 2003.

[8]van Dam, C. P., "Recent Experience with Different Methods of Drag Prediction," *Progress in Aerospace Sciences*, Vol. 35, No. 8, 1999, pp. 751–798.

[9]van der Vooren, J., and Slooff, J. W., "CFD-Based Drag Prediction; State of the Art, Theory, Prospects," Lectures Notes, AIAA Professional Studies Series, Course on Drag-Prediction and Measurement, 1990; also National Aerospace Lab., NLR Rept. TP-90247, Amsterdam, The Netherlands, 1990.

[10]Slooff, J. W., "Computational Drag Analysis and Minimization; Mission Impossible?," *Proceedings of the Aircraft Drag Prediction and Minimization Symposium*, AGARD R-723, Addendum 1, 1986.

[11]Oswatitsch, K., *Gas Dynamics*, Academic Press, New York, 1956, pp. 177–210.

[12]Chao, D. D., and van Dam, C. P., "Airfoil Drag and Decomposition," *Journal of Aircraft*, Vol. 36, No. 4, 1999, pp. 675–681.

[13]Giles, M. B., and Cummings, R. M., "Wake Integration for Three-Dimensional Flowfield Computations: Theoretical Development," *Journal of Aircraft*, Vol. 36, No. 2, 1999, pp. 357–365.

[14]Hunt, D. L., Cummings, R. M., and Giles, M. B., "Wake Integration for Three-Dimensional Flowfield Computations: Applications," *Journal of Aircraft*, Vol. 36, No. 2, 1999, pp. 366–373.

[15]Schmitt, V., and Destarac, D., "Recent Progress in Drag Prediction and Reduction for Civil Transport Aircraft at ONERA," AIAA Paper 98-0127, Jan. 1998.

[16]Destarac, D., "Far-Field/Near-Field Drag Balance and Applications of Drag Extraction in CFD," *CFD-Based Aircraft Drag Prediction and Reduction*, LS 2003-02, von Karman Inst. for Fluid Dynamics Lecture Series, von Karman Inst. for Fluid Dynamics, Rhode St-Genese, Belgium, 2003; also National Inst. of Aerospace, Hampton, VA, Nov. 2003.

[17]Paparone, L., and Tognaccini, R., "Computational Fluid Dynamics-Based Drag Based Drag Prediction and Decomposition," *AIAA Journal*, Vol. 41, No. 9, 2003, pp. 1647–1657.

[18]Tognaccini, R., "Methods for Drag Decomposition, Thrust–Drag Bookkeeping from CFD Calculations," *CFD-Based Aircraft Drag Prediction and Reduction*, LS 2003-02, von Karman Inst. for Fluid Dynamics Lecture Series, von Karman Inst. for Fluid Dynamics, Rhode St-Genese, Belgium, 2003; also National Inst. of Aerospace, Hampton, VA, Nov. 2003.

[19]Tognaccini, R., and Paparone, L., "Drag Breakdown and Drag/Thrust Bookkeeping from CFD Calculations," *Proceedings of the Workshop on EU-Research on Aerodynamic Engine/Aircraft Integration for Transport Aircraft*, German Aerospace Research Center, DLR, Brunswick, Germany, 2000, pp. 10-1, 10-14.

[20]Prandtl, L., "The Mechanics of Viscous Fluids," *Aerodynamic Theory*, edited by W. F. Durand, Vol. 3, Julius Springer, Berlin, 1935, p. 195.

[21]Martinelli, L., "Calculations of Viscous Flows with a Multigrid Method," Ph.D. Dissertation, Mechanical and Aerospace Engineering Dept., Princeton Univ., Princeton, NJ, Oct. 1987.

[22]Amato, M., Iaccarino, G., and Paparone, L., "Adaptive Local Grid Refinement for Multiblock Solvers," *Proceedings of the 20th Congress of ICAS*, Vol. 2, Reston, VA, 1996, pp. 1426–1433.

[23]Baldwin, B. S., and Lomax, H., "Thin Layer Approximation and Algebraic Model for Separated Turbulent Flows," AIAA Paper 78-257, Jan. 1978.

[24]Schlichting, H., *Boundary-Layer Theory*, 6th ed., McGraw Hill, New York, 1968, p. 599.

[25]Spalart, P. S., and Allmaras, S. R., "A One Equation Turbulence Model for Aerodynamics Flows," AIAA Paper 92-0439, Jan. 1992.